14th International Conference on Information Fusion
Chicago, Illinois, USA, July 5-8, 2011

Second Order Nonlinear Uncertainty Modeling in Strapdown Integration Using MEMS IMUs

Miao Zhang, Jeroen D. Hol, Laurens Slot, Henk Luinge
Xsens Technologies B.V.
Enschede, the Netherlands
Email: miao.zhang@xsens.com

***Abstract*—This paper applies the second order Taylor approximation to model the nonlinear uncertainty of acceleration rotation for MEMS based strapdown integration. Filtering solutions for tracking comprising inertial sensors require a good statistical modeling of the inertial measurements. The nonlinearity results in an umbrella-shape probability density distribution, and causes net downward vertical acceleration bias, which can not be estimated by traditional methods using only the first order approximation. This in turn leads to increasing vertical velocity and position errors after double integration which is significant for MEMS grade inertial sensors. Moreover, the analytical second order nonlinear term is applied in an extended Kalman filter (EKF) framework and compared with a normal EKF. The benefits of the method are demonstrated using a 3D MEMS IMU.**

Keywords: nonlinear filtering, state estimation, strapdown integration, MEMS inertial sensor.

I. Introduction

In recent years, micro electro mechanical system (MEMS) inertial sensors have been broadly used in navigation and tracking applications. MEMS inertial sensors usually need to be combined with other navigation systems to provide reliable long-term position estimates, e.g., Global Positioning System (GPS) for vehicle navigation [1], ultra wideband (UWB) for indoor positioning [2], and barometer for height estimate [3].

However, measurement noises and modeling errors will cause uncertainty in the calculation of orientation and acceleration. To solve this, a good modeling of the strapdown inertial integration needs to be given. The core of the strapdown inertial integration is acceleration rotation from body frame to navigation frame, which is a nonlinear mapping. The nonlinearity always brings a downward bias to vertical acceleration so that the integrals of that, i.e., vertical velocity and position will have increasing downward biases over time. The most traditional nonlinear filter in Bayesian framework is the extended Kalman filter (EKF), which applies the 1st order Taylor expansion to linearize nonlinear functions at a nominal trajectory. More advanced nonlinear filters are 2nd order EKF, unscented filter and particle filter [4]–[6], and so on. In order to understand the effect of the nonlinearity in strapdown inertial integration, here we derive the analytical 2nd order term in Taylor expansion and apply it in an EKF framework, called EKF2 (EKF1 to refer to a normal EKF). To focus on the nonlinear problem in inertial sensors, we run the prediction part of the filter within this work, which is in fact dead reckoning, to demonstrate the effect of different linearization ways, i.e., EKF1 and EKF2. It is expected that having a better linearization model for inertial sensors will benefit the overall estimation when integrated with other sensors.

The proposed approach is tested using an MEMS inertial measurement unit (IMU) consisting of a 3D rate gyroscope and a 3D accelerometer, as shown in Fig. 1. The results of dead reckoning using EKF1 and EKF2 show that the EKF2 provides better mean and covariance estimates of the acceleration rotation compared to that from EKF1. Especially the covariance estimate from EKF2 is more realistic than EKF1, i.e., consistent to the state estimate.

Figure 1: Xsens MEMS inertial sensor.

The rest of the paper is organized as follows: Section II introduces the strapdown inertial integration and the measurement model of MEMS inertial sensors. Section III addresses the acceleration rotation problem and the Taylor expansion is derived for this nonlinear mapping. Section IV explains the EKF2 algorithm and how it works for our problem. In section V, experimental results are analysed and demonstrate the benefits of EKF2. Finally conclusions are given in section VI.

II. Strapdown Inertial Integration

Strapdown inertial integration or dead reckoning [7], [8] calculates the current position from an initial position using measurements of angular velocity and specific force obtained by the inertial sensors, as shown in Fig. 2.

We first introduce the coordinate frames used in this paper:

- Navigation frame (n): This is a local geographic frame in which we want to navigate. That is, we want to know the

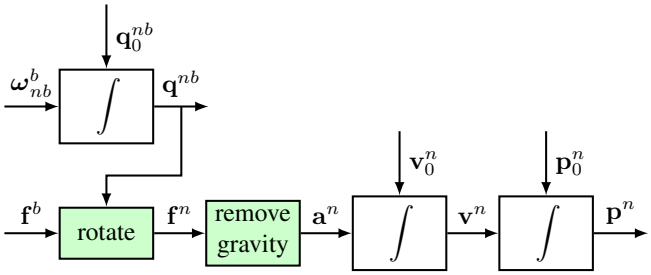

Figure 2: Strapdown inertial integration. Meaning of the symbols is explained in the text.

position and orientation of the sensor frame with respect to this frame. For most applications it is stationary with respect to the earth.

- Body frame (b): This is the coordinate frame of the moving IMU. Its origin is located in the center of the accelerometer axes, and it is aligned to the casing. All the inertial measurements are resolved in this coordinate system.

The measurements of inertial sensors and quantities in navigation are described with respect to these coordinates. In inertial sensors, accelerometers measure external specific force in body frame, denoted as $\mathbf{f}^b$. Gyroscopes measure angular velocity from body frame to inertial frame and expressed in the body frame. In order to keep the discussion simple, we apply correction terms which allow us to write the gyroscope measurement using the angular velocity from body frame to navigation frame and resolved in the body frame, $\boldsymbol{\omega}_{nb}^b$.

$$\mathbf{y}_{Gyr} = \boldsymbol{\omega}_{nb}^b + \mathbf{b}_\omega^b + \mathbf{e}_\omega^b \tag{1}$$

$$\mathbf{y}_{Acc} = \mathbf{f}^b + \mathbf{b}_a^b + \mathbf{e}_a^b = \mathbf{R}^{bn}(\mathbf{a}^n - \mathbf{g}^n) + \mathbf{b}_a^b + \mathbf{e}_a^b \tag{2}$$

where $\mathbf{R}^{bn}$ denotes the rotation matrix from navigation frame to body frame. $\mathbf{b}_\omega^b$ is the gyroscope bias and $\mathbf{b}_a^b$ is the accelerometer bias. They are slowly time-varying biases. $\mathbf{e}_\omega^b$ is the gyroscope measurement noise and $\mathbf{e}_a^b$ is the accelerometer measurement noise. They are assumed to be zero mean independent identically distributed (i.i.d.) Gaussian noises

$$e_\omega^b \sim \mathcal{N}(0, \sigma_{e_\omega}^2) \tag{3}$$

$$e_a^b \sim \mathcal{N}(0, \sigma_{e_a}^2) \tag{4}$$

It should be noticed that accelerometers do not measure acceleration directly, rather measure the so-called external specific force to which the acceleration $\mathbf{a}^n$ as well as the earth's gravitational field $\mathbf{g}^n$ contribute, as shown in Eq. (2). Therefore, the strapdown inertial integration as illustrated in Fig. 2 has the following procedure: The orientation $\mathbf{q}^{nb}$ is calculated by integrating the angular velocity, $\boldsymbol{\omega}_{nb}^b$, measured by gyroscopes. Then the global acceleration is obtained by rotating the specific force measured from accelerometers, $\mathbf{f}^b$, and correcting the gravity. Finally the velocity and position relative to an initial point, $\mathbf{v}^n$ and $\mathbf{p}^n$, are determined by the integration of the acceleration, $\mathbf{a}^n$.

III. Nonlinear Problem of Acceleration Rotation

The core of the strapdown integration is the acceleration rotation, rotating the specific force measured by accelerometers to the navigation frame according to the orientation, as shown in Fig. 2. It can be described by

$$\mathbf{a}_k^n = \mathbf{q}_k^{nb} \odot \mathbf{f}_k^b \odot \mathbf{q}_k^{nb,c} + \mathbf{g}^n \tag{5}$$

The orientation is represented by quaternion [9], e.g., $\mathbf{q}^{nb}$ represents the rotation from body frame to the navigation frame. The vector rotation is done by quaternion multiplication, $\odot$, and the superscript c is the quaternion conjugation operation.

Equation (5) is a nonlinear function. It is problematic in the strapdown integration since it always results in a downward bias in the vertical acceleration. The probability density function of the rotated acceleration is not a Gaussian shape, but rather like an umbrella. Hence, we name this nonlinear problem 'umbrella problem'. In Fig. 3, the arrow is an acceleration vector to be estimated, but the rotated acceleration (the dots in the figure) by an orientation error, which is Gaussian distributed, are like an umbrella. The mean of the rotated acceleration in vertical direction is always downward.

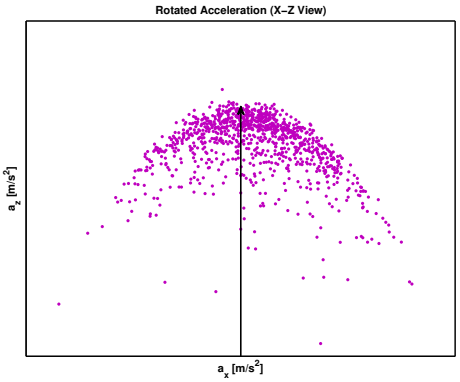

Figure 3: Umbrella problem illustration (X-Z view): arrow is a true acceleration vector, dots are the rotated acceleration with uncertain orientation errors.

Figure 4 illustrates this downward bias for one sample. Assume that $\hat{\mathbf{g}}$ is the estimate of vector $\mathbf{g}$ after rotating, it has errors because there is an orientation uncertainty θ. The vertical error e can be roughly calculated by Taylor expansion so that $e = ||\mathbf{g}||\,(1 - \cos(\theta)) \approx \frac{1}{2}\,||\mathbf{g}||\,\theta^2$, and this error is always downward. This bias caused by the nonlinearity of acceleration rotation will be integrated to the velocity and position in vertical direction and grow fast with time.

The most common nonlinear filtering approach is to linearize the nonlinear functions using the 1st order Taylor expansion and then to apply Kalman filter. However, for the problem we point out in this paper, the 1st order Taylor expansion cannot model the downward bias due to the nonlinearity and we need a higher order nonlinear term to solve it. For

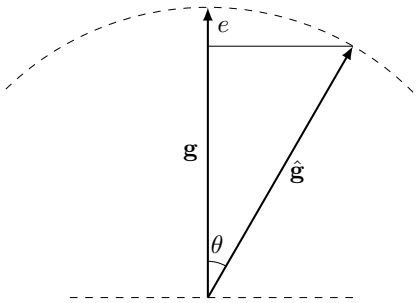

Figure 4: Simplified explanation of 'umbrella problem'. Within the strapdown integration, the acceleration is computed by adding the gravity to the specific force (Eq. 5). Any orientation error will therefore result in a downward acceleration error.

simplicity, in the following of this section, we remove the time subscript k.

The orientation $\mathbf{q}^{nb}$ can be split into a nominal orientation $\bar{\mathbf{q}}^{nb}$ and an orientation error $\boldsymbol{\theta}^b$

$$\mathbf{q}^{nb} \triangleq \bar{\mathbf{q}}^{nb} \odot \exp(-\tfrac{1}{2}\boldsymbol{\theta}^b) \tag{6}$$

where $\bar{\mathbf{q}}^{nb}$ is the linearization point for the orientation and $\boldsymbol{\theta}^b$ denotes orientation error in helical axis. $\exp(\cdot)$ denotes quaternion exponential, which is defined as

$$\exp(0, \mathbf{v}) \triangleq \left(\cos||\mathbf{v}||\,, \tfrac{\mathbf{v}}{||\mathbf{v}||}\sin||\mathbf{v}||\right) \tag{7}$$

where $\mathbf{v}$ represents a vector. The orientation error is selected for the purpose of having a local Euclidean description of the orientation without constraints. Then the acceleration rotation, Eq. (5), can be formulated as a nonlinear function of orientation error $\boldsymbol{\theta}^b$

$$\begin{aligned}\mathbf{a}^n &\triangleq \mathbf{f}(\boldsymbol{\theta}^b) &(8)\\ &= \bar{\mathbf{q}}^{nb} \odot \exp(-\tfrac{1}{2}\boldsymbol{\theta}^b) \odot \mathbf{f}^b \odot \exp(-\tfrac{1}{2}\boldsymbol{\theta}^b)^c \odot \bar{\mathbf{q}}^{nb,c} + \mathbf{g}^n &(9)\\ &= \bar{\mathbf{R}}^{nb} \cdot \exp(-\tfrac{1}{2}\boldsymbol{\theta}^b) \odot \mathbf{f}^b \odot \exp(-\tfrac{1}{2}\boldsymbol{\theta}^b)^c + \mathbf{g}^n &(10)\end{aligned}$$

The Taylor expansion is

$$\begin{aligned}\mathbf{f}(\mathbf{x}) =& \mathbf{f}(\bar{\mathbf{x}}) + [\mathbf{D}_{\mathbf{x}}\mathbf{f}]_{\bar{\mathbf{x}}}(\mathbf{x}-\bar{\mathbf{x}})\\ &+\tfrac{1}{2}(\mathbf{I}\otimes(\mathbf{x}-\bar{\mathbf{x}})^T)[\mathbf{H}_{\mathbf{xx}}\mathbf{f}]_{\bar{\mathbf{x}}}(\mathbf{x}-\bar{\mathbf{x}}) + \text{hot.}\end{aligned} \tag{11}$$

where $[\mathbf{D}_{\mathbf{x}}\mathbf{f}]_{\bar{\mathbf{x}}}$ denotes the Jacobian matrix of the nonlinear functions $\mathbf{f}(\mathbf{x})$ with respect to $\mathbf{x}$ and $[\mathbf{H}_{\mathbf{xx}}\mathbf{f}]_{\bar{\mathbf{x}}}$ denotes the Hessian matrix. They are evaluated at a linearization point $\bar{\mathbf{x}}$. The symbol $\otimes$ is the Kronecker product. The mathematics of matrix derivatives can be referred to in [10]. Therefore, the 1st order Taylor linearization of the acceleration rotation, $\mathbf{f}(\boldsymbol{\theta}^b)$, can be derived at a linearization point $\bar{\boldsymbol{\theta}}^b = \mathbf{0}$

$$\mathbf{f}^{1st}(\boldsymbol{\theta}^b) = \underbrace{\bar{\mathbf{R}}^{nb}\mathbf{f}^b + \mathbf{g}^n}_{\mathbf{f}(\bar{\boldsymbol{\theta}}^b)} + \underbrace{[\mathbf{D}_{\boldsymbol{\theta}}\mathbf{f}]_{\bar{\boldsymbol{\theta}}^b}\cdot\boldsymbol{\theta}^b}_{1^{\text{st}}\text{ order term}} \tag{12}$$

and the 2nd order linearization will be

$$\begin{aligned}\mathbf{f}^{2nd}(\boldsymbol{\theta}^b) =& \bar{\mathbf{R}}^{nb}\mathbf{f}^b + \mathbf{g}^n + [\mathbf{D}_{\boldsymbol{\theta}}\mathbf{f}]_{\bar{\boldsymbol{\theta}}^b}\cdot\boldsymbol{\theta}^b\\ &+\underbrace{\tfrac{1}{2}(\mathbf{I}\otimes(\boldsymbol{\theta}^b)^T)[\mathbf{H}_{\boldsymbol{\theta}\boldsymbol{\theta}}\mathbf{f}]_{\bar{\boldsymbol{\theta}}^b}\boldsymbol{\theta}^b}_{2^{\text{nd}}\text{ order term}}\end{aligned} \tag{13}$$

Assume that $\boldsymbol{\theta}^b$ is a random variable of i.i.d. Gaussian, $\boldsymbol{\theta}^b \sim \mathcal{N}(\boldsymbol{\mu}_{\boldsymbol{\theta}^b}, \boldsymbol{\Sigma}_{\boldsymbol{\theta}^b})$, and the linearization point is chosen at $\bar{\boldsymbol{\theta}}^b = \boldsymbol{\mu}_{\boldsymbol{\theta}^b} = \mathbf{0}$. Since $\mathbf{f}^b$ is the measurement from accelerometers, it is assumed to be white Gaussian, $\mathbf{f}^b \sim \mathcal{N}(\boldsymbol{\mu}_{\mathbf{f}^b}, \boldsymbol{\Sigma}_{\mathbf{f}^b})$. Then the mean and covariance of the 1st order Taylor linearization, Eq. (12), are

$$\mathrm{E}\{\mathbf{f}^{1st}\} = \bar{\mathbf{R}}^{nb}\boldsymbol{\mu}_{\mathbf{f}^b} + \mathbf{g}^n \tag{14}$$

$$\mathrm{Cov}\{\mathbf{f}^{1st}\} = [\mathbf{D}_{\boldsymbol{\theta}}\mathbf{f}]_{\bar{\boldsymbol{\theta}}^b}\boldsymbol{\Sigma}_{\boldsymbol{\theta}^b}[\mathbf{D}_{\boldsymbol{\theta}}\mathbf{f}]^T_{\bar{\boldsymbol{\theta}}^b} + \bar{\mathbf{R}}^{nb}\boldsymbol{\Sigma}_{\mathbf{f}^b}\bar{\mathbf{R}}^{nb,T} \tag{15}$$

Similarly, the mean and covariance for the 2nd order Taylor linearization, Eq. (13), are

$$\begin{aligned}\mathrm{E}\{\mathbf{f}^{2nd}\} =& \bar{\mathbf{R}}^{nb}\boldsymbol{\mu}_{\mathbf{f}^b} + \mathbf{g}^n\\ &+\tfrac{1}{2}\left[\mathrm{tr}([\mathbf{H}_{\boldsymbol{\theta}\boldsymbol{\theta}}\mathbf{f}]_{\bar{\boldsymbol{\theta}}^b,i}\boldsymbol{\Sigma}_{\boldsymbol{\theta}^b})\right]_i\end{aligned} \tag{16}$$

$$\begin{aligned}\mathrm{Cov}\{\mathbf{f}^{2nd}\} =& [\mathbf{D}_{\boldsymbol{\theta}}\mathbf{f}]_{\bar{\boldsymbol{\theta}}^b}\boldsymbol{\Sigma}_{\boldsymbol{\theta}^b}[\mathbf{D}_{\boldsymbol{\theta}}\mathbf{f}]^T_{\bar{\boldsymbol{\theta}}^b} + \bar{\mathbf{R}}^{nb}\boldsymbol{\Sigma}_{\mathbf{f}^b}\bar{\mathbf{R}}^{nb,T}\\ &+\tfrac{1}{2}\left[\mathrm{tr}([\mathbf{H}_{\boldsymbol{\theta}\boldsymbol{\theta}}\mathbf{f}]_{\bar{\boldsymbol{\theta}}^b,i}\boldsymbol{\Sigma}_{\boldsymbol{\theta}^b}[\mathbf{H}_{\boldsymbol{\theta}\boldsymbol{\theta}}\mathbf{f}]_{\bar{\boldsymbol{\theta}}^b,j}\boldsymbol{\Sigma}_{\boldsymbol{\theta}^b})\right]_{ij}\end{aligned} \tag{17}$$

where $\mathrm{tr}(\cdot)$ is the matrix trace operation. $[\mathbf{x}_i]_i$ denotes a vector whose i^{th} element is $\mathbf{x}_i$, and $[\mathbf{x}_{ij}]_{ij}$ denotes a matrix whose ij^{th} element is $\mathbf{x}_{ij}$. Comparing the mean and covariance of 2nd order linearization with those of the 1st order, an extra term is added and it represents the downward bias caused by the nonlinearity of acceleration rotation. In addition, this term in the mean as well as in the covariance depends on the uncertainty of the orientation, $\boldsymbol{\Sigma}_{\boldsymbol{\theta}^b}$.

IV. Nonlinearity Modeling in EKF

A. EKF2 Algorithm

After deriving the 1st and 2nd order Taylor linearization expansion for the highly nonlinear mapping of acceleration rotation, a natural choice for filtering is EKF. In real applications, the 1st order EKF is the most general approach and in fact it works well when the model is almost linear or the signal noise ratio (SNR) is high [4]. For our problem, it means that the higher order nonlinear term can be neglected when the uncertainty of the orientation is sufficiently small. However, in MEMS inertial sensors, this uncertainty cannot be neglected and it grows with respect to the dead reckoning time. In the following first we discuss a general EKF algorithm.

A discrete-time nonlinear state space model can be written as

$$\mathbf{x}_{k+1} = \mathbf{f}(\mathbf{x}_k, \mathbf{w}_k) \tag{18}$$

$$\mathbf{y}_k = \mathbf{h}(\mathbf{x}_k, \mathbf{v}_k) \tag{19}$$

where

$$\mathbf{w}_k \sim \mathcal{N}(\mathbf{0}, \mathbf{Q}_k) \tag{20}$$

$$\mathbf{v}_k \sim \mathcal{N}(\mathbf{0}, \mathbf{R}_k) \tag{21}$$

Then an 2nd order EKF (EKF2) [4], [11] based on the 2nd order Taylor expansion is given by

Initialization:

$$\hat{\mathbf{x}}_0^+ = \mathrm{E}\{\mathbf{x}_0\} \tag{22}$$
$$\mathbf{P}_0^+ = \mathrm{Cov}\{\mathbf{x}_0\} \tag{23}$$

Prediction:

$$\hat{\mathbf{x}}_k^- = \mathbf{f}(\hat{\mathbf{x}}_{k-1}^+) + \tfrac{1}{2}\left[\mathrm{tr}\left(\mathbf{f}''_{i,\mathbf{x}}(\hat{\mathbf{x}}_{k-1}^+)\mathbf{P}_{k-1}^+\right)\right]_i \tag{24}$$
$$\mathbf{P}_k^- = \mathbf{f}'_{\mathbf{x}}(\hat{\mathbf{x}}_{k-1}^+)\mathbf{P}_{k-1}^+\mathbf{f}'_{\mathbf{x}}(\hat{\mathbf{x}}_{k-1}^+) + \mathbf{Q}_k + \tfrac{1}{2}\left[\mathrm{tr}\left(\mathbf{f}''_{i,\mathbf{x}}(\hat{\mathbf{x}}_{k-1}^+)\mathbf{P}_{k-1}^+\mathbf{f}''_{j,\mathbf{x}}(\hat{\mathbf{x}}_{k-1}^+)\mathbf{P}_{k-1}^+\right)\right]_{ij} \tag{25}$$

Correction:

$$\mathbf{S}_k = \mathbf{h}'_{\mathbf{x}}(\hat{\mathbf{x}}_k^-)\mathbf{P}_k^-\left(\mathbf{h}'_{\mathbf{x}}(\hat{\mathbf{x}}_k^-)\right)^T + \mathbf{R}_k + \tfrac{1}{2}\left[\mathrm{tr}\left(\mathbf{h}''_{i,\mathbf{x}}(\hat{\mathbf{x}}_k^-)\mathbf{P}_k^-\mathbf{h}''_{j,\mathbf{x}}(\hat{\mathbf{x}}_k^-)\mathbf{P}_k^-\right)\right]_{ij} \tag{26}$$
$$\mathbf{K}_k = \mathbf{P}_k^-\left(\mathbf{h}'_{\mathbf{x}}(\hat{\mathbf{x}}_k^-)\right)^T(\mathbf{S}_k)^{-1} \tag{27}$$
$$\mathbf{r}_k = \mathbf{y}_k - \mathbf{h}(\hat{\mathbf{x}}_k^-) - \tfrac{1}{2}\left[\mathrm{tr}\left(\mathbf{h}''_{i,\mathbf{x}}(\hat{\mathbf{x}}_k^-)\mathbf{P}_k^-\right)\right]_i \tag{28}$$
$$\hat{\mathbf{x}}_k^+ = \hat{\mathbf{x}}_k^- + \mathbf{K}_k\mathbf{r}_k \tag{29}$$
$$\mathbf{P}_k^+ = \mathbf{P}_k^- - \mathbf{P}_k^-\left(\mathbf{h}'_{\mathbf{x}}(\hat{\mathbf{x}}_k^-)\right)^T(\mathbf{S}_k)^{-1}\mathbf{h}'_{\mathbf{x}}(\hat{\mathbf{x}}_k^-)\mathbf{P}_k^- \tag{30}$$

where $\mathbf{f}'_{\mathbf{x}}, \mathbf{h}'_{\mathbf{x}}$ denote the Jacobian matrix and $\mathbf{f}''_{\mathbf{x}}, \mathbf{h}''_{\mathbf{x}}$ represent the Hessian matrix. Comparing the prediction part of EKF2 algorithm with Eqs. (16) and (17), the EKF2 just estimates the mean and covariance of the 2nd order Taylor expansion. When only the 1st order Taylor linearization is used, i.e., a normal EKF (EKF1) is applied, the Hessians $\mathbf{f}''_{\mathbf{x}}, \mathbf{h}''_{\mathbf{x}}$ are set to zero. The additional term of EKF2 as compared to EKF1 models the nonlinearity. When the 2nd order nonlinear term is not trivial, EKF1 will fail.

B. Nonlinear Estimation Based on Simulation

As is well known, Kalman filters estimate only the mean and the covariance of the states instead of the entire probability density function. Figure 5 illustrates the performance of EKF1, EKF2 and particle filter for the addressed nonlinear problem based on a simulation. In the prediction part, the orientation evolves with respect to time and the acceleration rotates at each time, as shown in Fig. 2. For simplicity, the correction part of the filter is built by a known acceleration measurement with noise. The specific force and orientation error are assumed zero mean white Gaussian distributed.

In Fig. 5, the red star represents a real acceleration. In each time sample, zero mean white Gaussian noises are added to the orientation error and specific force. These uncertainties will cause the umbrella effect, as shown in Fig. 5a. The blue dots are the predicted acceleration of EKF1 and the green circles are those from EKF2. Each dot represents one sample. The black asterisks are the mean outputs of a particle filter. The blue, green and black stars and the corresponding ellipses are the estimates and 99.5% confidence ellipses for different nonlinear filters in a specific sample. It is observed that the predicted estimates of the EKF2 (green circles) are lower compared with those of the EKF1 (blue dots) and are comparative with those of the particle filter. From the first thought we

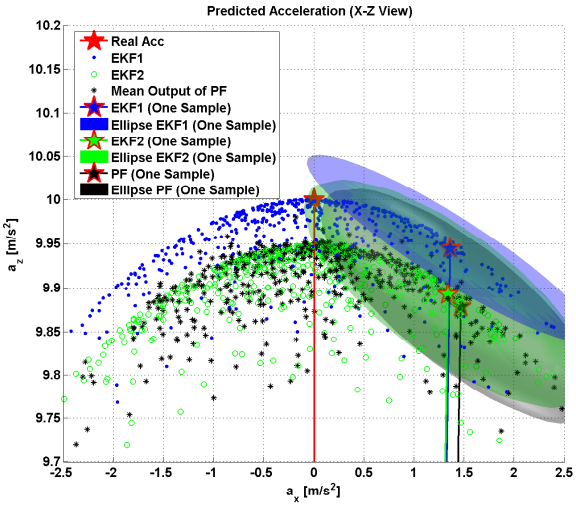

(a) Predicted Acceleration

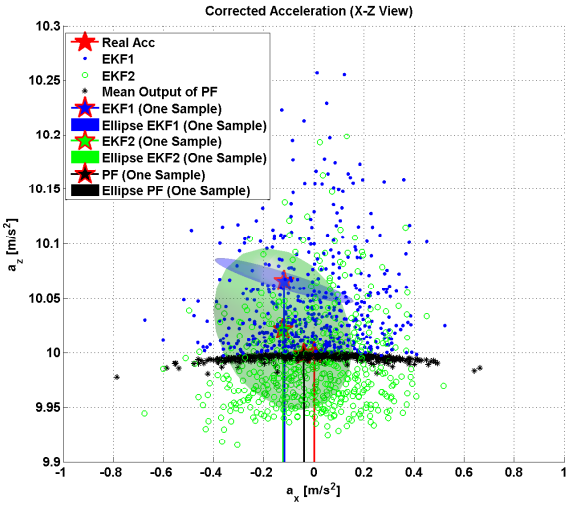

(b) Corrected Acceleration

Figure 5: Nonlinear filter performance: the red star is the real acceleration, blue dots are the estimates from EKF1, green circles are the estimates from EKF2, black asterisks are the mean outputs from a particle filter. The blue, green and black stars are the estimates of different filters at one sample and the corresponding ellipses represents the corresponding 99.5% confidence ellipses at this sample.

expected that the estimate of EKF2 could compensate the bias and be more close to the real acceleration. However, the EKF only gives the mean and the covariance estimate of the real distribution, i.e., a single point (blue or green) represents the mean from EKF1 or EKF2 in that time sample. Hence, EKF2 estimates the downward bias of the umbrella problem more correctly as compared to EKF1. Especially

when we combine the mean and covariance estimate, the ellipses, the real acceleration is within the confidence area of EKF2 whereas this is not the case for EKF1. Therefore, the predicted estimate of EKF2 provides a more correct mean as well as covariance estimate. Moreover, the performance of EKF2 is close to that of the particle filter, which means that the EKF2 can model the nonlinearity very well. Figure 5b shows the performance after correction. It is demonstrated that the EKF1 estimate has always a bias in height whereas the EKF2 provides a much better estimate with a reasonable covariance estimate.

Usually, a navigation or tracking solution combines inertial sensors and other systems. For example, in [2], the inertial system serves as a process model and a UWB system is applied in the correction part of the filter. In order to focus on the nonlinear problem of strapdown integration, in the following experiment we only consider the prediction part of the Kalman filter, i.e., only the nonlinearity of the acceleration rotation is considered. In practice, the dead reckoning is very important in the fusion since the inertial sensors have high frequency data and other aiding sources usually provide relatively lower frequency data. So that a good dead reckoning output with realistic covariance is necessary.

V. Experimental Results

A. Inertial Measurements

The addressed nonlinearity problem is tested using an MEMS inertial sensor including 3D gyroscopes and 3D accelerometers, as shown in Fig. 1. The sensor unit is mounted on a stationary table, and 3 hours stationary data are measured at a frequency of 200 Hz. Therefore, we have ground truth for evaluating the performance of the filters.

B. Process Model

As given in Eq. (1) and (2), the inertial measurements include slowly time-varying biases. They should also be in the state vector to be estimated. Therefore, a discrete-time nonlinear state-space model can be built and the state vector consists of orientations, gyroscope biases, accelerometer biases, 3D velocities and 3D positions

$$\mathbf{q}^{nb}_{k+1} = \mathbf{q}^{nb}_{k} \odot \exp(\tfrac{T}{2}\boldsymbol{\omega}^{b}_{nb,k}) \tag{31}$$

$$\mathbf{b}^{b}_{\omega,k} = \mathbf{b}^{b}_{\omega,k-1} + \mathbf{w}_{b_\omega} \tag{32}$$

$$\mathbf{b}^{b}_{a,k} = \mathbf{b}^{b}_{a,k-1} + \mathbf{w}_{b_a} \tag{33}$$

$$\mathbf{v}^{n}_{k} = \mathbf{v}^{n}_{k-1} + T \cdot \mathbf{a}^{n}_{k-1} + \mathbf{w}_{v} \tag{34}$$

$$\mathbf{p}^{n}_{k} = \mathbf{p}^{n}_{k-1} + T \cdot \mathbf{v}^{n}_{k-1} + \tfrac{T^2}{2} \cdot \mathbf{a}^{n}_{k-1} + \mathbf{w}_{p} \tag{35}$$

where $\mathbf{x} = \begin{bmatrix}\mathbf{q}^{nb,T} & \mathbf{b}^{b,T}_{\omega} & \mathbf{b}^{b,T}_{a} & \mathbf{v}^{n,T} & \mathbf{p}^{n,T}\end{bmatrix}^T$, and T in the process model is the sampling interval. $\mathbf{a}^{n}_{k}$ results from the highly nonlinear mapping, the rotation of acceleration, as calculated in Eq. (8). To focus on this nonlinear problem, here only the process model is given. As introduced earlier, the measurement part for a navigation and tracking scheme can be different aiding sensors, e.g., barometers, which is not in the scope of this paper.

C. Dead Reckoning Test

To examine the different linearization approaches for the addressed nonlinear problem, we test EKF1 and EKF2 using the above process model. The strapdown integration starts with initial orientation uncertainty of 1 degree, and other initial states are assumed to be known exactly. 200 iterations are run, i.e., 1 second dead reckoning. Then this procedure is repeated 5000 times for different datasets so that the statistics of the dead reckoning can be obtained.

Figure 6 shows the height and covariance estimate from EKF1 and EKF2, respectively. To show the results clearly, here 100 dead reckoning samples are shown in the plot. It should be noted that the acceleration in navigation frame is $\begin{bmatrix}0 & 0 & 0\end{bmatrix}^T$ since we have stationary data. The true mean of the rotated acceleration is not zero in vertical direction. From the plot it is observed that both outputs from EKF1 and EKF2 are lower than zero. The EKF2 provides even lower estimate in vertical direction compared to the EKF1. This result is consistent with the simulation in Fig. 5a.

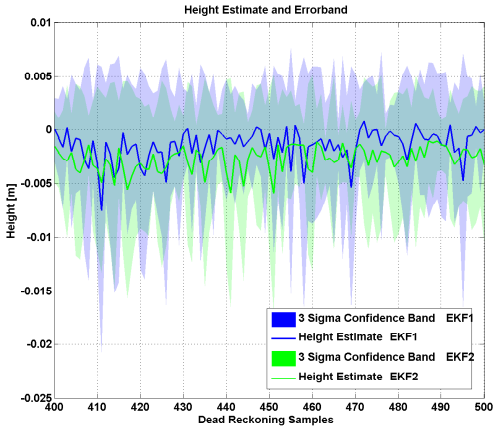

Figure 6: Height estimate and covariance.

D. Evaluating the Covariance Estimate

We are interested in the covariance estimate since a good estimator should provide both the correct mean and the correct covariance from the prediction, by which the correction part of the filter can work properly when we combine inertial measurements with other sensors. In the following, we choose a normalized error as the criteria to evaluate the estimate. Assume the estimate after dead reckoning is defined as $\mathbf{e}_{\mathbf{x}}$, which also represents the estimated error since it is a stationary trial, and the covariance output is defined as $\mathbf{P}$. We can define a normalized error (NE) and a normalized error squared (NES) similar to the standard quantities for evaluating the performance of a filter, normalized residual (NR) and normalized innovation squared (NIS). For a good estimator, NE should be a multiple-dimensional normal Gaussian distribution, and

NES should be a chi-square distribution.

$$\text{NE} \triangleq \mathbf{e}_{\mathbf{x}}^T \cdot \mathbf{P}^{-\frac{1}{2}} \sim \mathcal{N}(\mathbf{0}, \mathbf{1}) \tag{36}$$

$$\text{NES} \triangleq \mathbf{e}_{\mathbf{x}}^T \cdot \mathbf{P}^{-1} \cdot \mathbf{e}_{\mathbf{x}} \sim \chi_k^2 \tag{37}$$

where k is the freedom of the chi-square distribution and it is the dimension of the state vector. Here NE and NES are evaluated in the state elements of orientation, velocity and position, so that NES should be a chi-square distribution with 9 degrees of freedom.

In Fig. 7, the normalized histogram of the orientation elements in NE is plotted with a normal Gaussian distribution. Since the same 1st order linearization model for the orientation integration is used in both of the EKF1 and EKF2, the same performance for the orientation elements is obtained for both filters. So that Fig. 7 represents both the results from EKF1 and EKF2. The histogram is plotted based on the 5000 dead reckoning trials, which uses different real datasets. It is observed that each of the orientation elements in NE complies with the normal Gaussian distribution. This result demonstrates that the EKF1 model for the orientation evolution with time using gyroscope measurements is a good model.

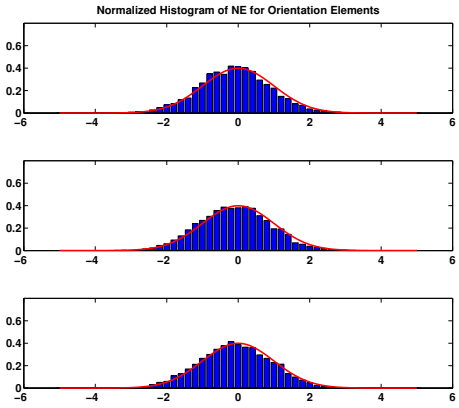

Figure 7: Normalized histogram of NE for the orientation elements (same for EKF1 and EKF2): red plots are normal Gaussian distributions, blue plots are normalized histogram of the orientation elements in NE.

Figure 8 shows the normalized histogram of the position elements in the NE from EKF1 and EKF2, respectively. There are minor differences between the two filters at the position x and y elements. For the position z element, it is observed that EKF1 has a biased error, whereas the EKF2 provides a better estimate, which is more close to the normal Gaussian distribution. Recall Fig. 4, the downward bias in the vertical acceleration will cause the bias in the vertical position. Figure 8 proves that EKF1 does not solve this problem, whereas the EKF2 can fix it by providing a better mean estimate and corresponding covariance estimate. It can be expected that by modeling the nonlinearity of acceleration rotation, correct height estimate can be obtained by EKF2.

For more clear about the benefit of EKF2, the NES quantity is further checked as shown in Fig. 9. By the comparison of EKF1 and EKF2, the NES from EKF2 looks more like a chi-square distribution than the NES from EKF1. It shows that the covariance estimate from EKF1 does not match the mean estimate error, i.e., the EKF1 can not model the downward bias due to the nonlinearity correctly, whereas the EKF2 has a better estimate for the nonlinear problem of acceleration rotation.

Moreover, to evaluate the covariance estimate, noncredibility Indices (NIC) [12] can be calculated as

$$\text{NCI} \triangleq \frac{10}{M} \sum_{i=1}^{M} \log_{10} \left[\frac{\mathbf{e}_{\mathbf{x}}^T \mathbf{P}^{-1} \mathbf{e}_{\mathbf{x}}}{\mathbf{e}_{\mathbf{x}}^T \mathbf{\Sigma}^{-1} \mathbf{e}_{\mathbf{x}}} \right]_i \tag{38}$$

$$= \frac{10}{M} \sum_{i=1}^{M} \log_{10} \left[\mathbf{e}_{\mathbf{x}}^T \mathbf{P}^{-1} \mathbf{e}_{\mathbf{x}} \right]_i - \frac{10}{M} \sum_{i=1}^{M} \log_{10} \left[\mathbf{e}_{\mathbf{x}}^T \mathbf{\Sigma}^{-1} \mathbf{e}_{\mathbf{x}} \right]_i \tag{39}$$

where $\mathbf{\Sigma}$ is the true covariance of the estimate error, which is approximated by the 5000 samples due to the known stationary trial. M is the number of samples. As shown in Eq. (39), the NCI should be approximated to zero when the NES of the filter is close to the true error, which means the estimator is perfectly credible. The NCI for EKF1 is equal to 2.3 and the NCI for EKF2 is 0.3, which demonstrates EKF2 has a significant improvement compared to the EKF1.

VI. Conclusions

In this paper, we address the nonlinear problem of acceleration rotation in strapdown inertial integration. The estimate using the traditional 1st order linearization does not model the downward bias in the vertical acceleration caused by this nonlinearity. This brings fast-growing biases in the vertical velocity and position after integration. It is very important to model this nonlinearity to have a realistic model of inertial sensors to be able to perform accurate height tracking. We propose to use the 2nd order Taylor expansion to approximate this nonlinearity and apply an EKF2 filter. Moreover, traditional Kalman filter solutions such as in EKF1 the error propagation is separated from the state propagation. Whereas in EKF2, the state propagation depends on the error covariances, which makes the error modeling more important. A dead reckoning test using stationary measurements from an MEMS inertial sensor demonstrates that EKF2 can better model this nonlinear mapping.

In the future, more advanced nonlinear filters can be considered, e.g., particle filter, and the nonlinearity modeling proposed in this paper can be applied in different fusion applications to provide a good position estimate.

Acknowledgement

The research leading to these results has received funding from the EU's Seventh Framework Programme under grant agreement no. 238710. The research has been carried out in the MC IMPULSE project: https://mcimpulse.isy.liu.se.

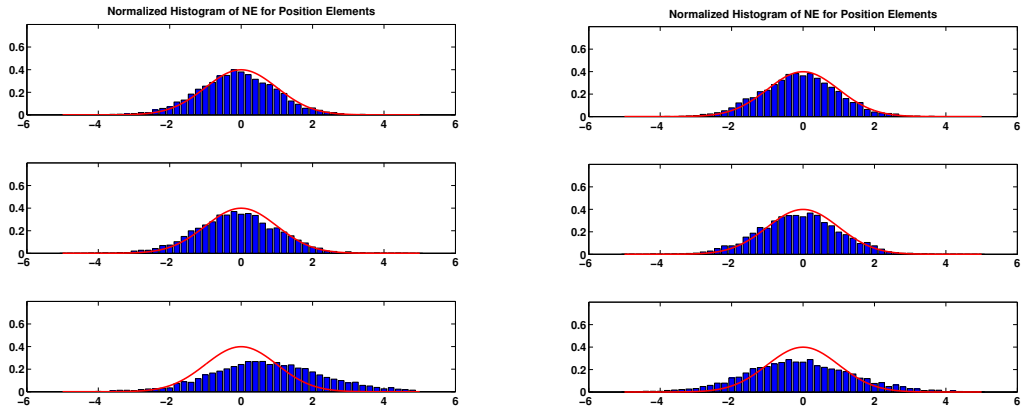

(a) EKF1 (b) EKF2

Figure 8: Normalized histogram of NE for the position elements: red plots are normal Gaussian distributions, blue plots are normalized histogram of the position elements in NE.

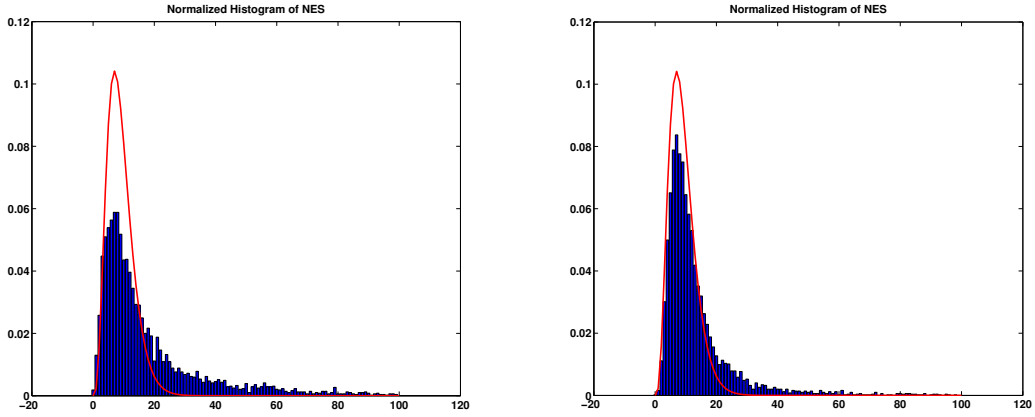

(a) EKF1 (b) EKF2

Figure 9: Normalized histogram of NES: red plots are a chi-square distribution with 9 dimension of freedom, blue plots are normalized histograms of NES including orientation, velocity and position.

REFERENCES

[1] A. Vydhyanathan, M. Kok, and K. L. Johnson, "A low-cost navigation system: high dynamic flight test results," in *Proc. of The European Navigation Conference on Global Navigation Satellite Systems*, Braunschweig, Germany, Oct. 2010.

[2] J. D. Hol, F. Dijkstra, H. Luinge, and T. B. Schön, "Tightly coupled UWB/IMU pose estimation," in *Proc. of IEEE International Conference on Ultra-Wideband 2009*, Vancouver, Canada, Sep. 2009, pp. 688–692.

[3] M. Tanigawa, H. Luinge, L. Schipper, and P. Slycke, "Drift-free dynamic height sensor using MEMS IMU aided by MEMS pressure sensor," in *Proc. of 5th Workshop on Positioning, Navigation and Communication, 2008*, Hannover, Germany, Mar. 2008, pp. 191–196.

[4] F. Gustafsson, *Statistical Sensor Fusion*. Studentlitteratur, 2010.

[5] D. Simon, *Optimal State Estimation: Kalman HInfinity, and Nonlinear Approaches*. John Wiley & Sons, 2006.

[6] B. Ristic, S. Arulampalam, and N. Gordon, *Beyond Kalman Filter: Particle Filters for Tracking Applications*. Artech House Radar Library, 2004.

[7] D. H. Titterton and J. L. Weston, *Strapdown Inertial Navigation Technology*. Peter Peregrinus Ltd., 1997, IEE radar, sonar, navigation and avionics series.

[8] J. E. Bortz, "A new mathematical formulation for strapdown inertial navigation," *IEEE Transactions on Aerospace and Electronic Systems*, vol. 7, no. 1, pp. 61–66, 1971.

[9] M. D. Shuster, "A survey of attitude representations," *The journal of the Astronautical Sciences*, vol. 41, no. 4, pp. 439–517, Oct. 1993.

[10] J. R. Magnus and H. Neudecker, *Matrix Differential Calculus with Applications in Statistics and Econometrics*. John Wiley & Sons, 1999.

[11] P. S. Maybeck, *Stochastic Models, Estimation, and Control*. Academic Press, 1979, vol. 2.

[12] X. Li and Z. Zhao, "Measuring estimator's credibility: Noncredibility index," in *Proc. of The 9th International Conference on Information Fusion*, Florence, Italy, Jul. 2006.